Antiferromagnetic domains and superconductivity in UPt_3

Matthias J. Graf
Theoretical Division, Los Alamos National Laboratory, Los Alamos, New Mexico 87545

Daryl W. Hess
Center for Computational Materials Science, Naval Research Laboratory, Washington, D.C. 20375-5345

(Received 14 August 2000; published 23 February 2001)

We explore the response of an unconventional superconductor to spatially inhomogeneous antiferromagnetism (SIAFM). Symmetry allows the superconducting order parameter in the *E*-representation models for UPt_3 to couple directly to the antiferromagnetic (AFM) order parameter. The Ginzburg-Landau equations for coupled superconductivity and SIAFM are solved numerically for two possible SIAFM configurations: Model I, abutting antiferromagnetic domains of uniform size; and Model II, quenched random disorder of ''nanodomains'' in a uniform AFM background. We discuss the contributions to the free energy, specific heat, and order parameter for these models. Neither model provides a satisfactory account of experiment, but results from the two models differ significantly. Our results demonstrate that the response of an E_{2u} superconductor to SIAFM is strongly dependent on the spatial dependence of AFM order; no conclusion can be drawn regarding the compatibility of E_{2u} superconductivity with UPt_3 that is independent of assumptions on the spatial dependence of antiferromagnetism.

DOI: 10.1103/PhysRevB.63.134502 PACS number(s): 74.70.Tx, 74.20.−z, 74.80.−g, 74.25.Dw

I. INTRODUCTION

The nature of the spatially inhomogeneous small-moment antiferromagnetism observed in neutron-scattering experiments[1–3] below $T_N \sim 6$ K and its interaction with superconductivity ($T_c \sim 0.5$ K) remain central issues in determining the symmetry of the superconducting order parameter of UPt_3. The unusual H-T phase diagram[4,5] at ambient pressure apparently shows three superconducting phases in the mixed state and two Meissner phases. Experimental studies using hydrostatic[3] and uniaxial[6] pressure reveal the existence of a critical pressure above which the zero-field transition splitting disappears. This complex phase diagram strongly suggests that superconductivity in this heavy-electron material is unconventional and has provided motivation for much theoretical work.[7–12] Proposed theories range from odd-in-frequency pairing[11] to multicomponent order parameters. The latter may belong to a single multidimensional representation of the symmetry group (see Refs. 7 and 8 for reviews), or they may belong to different representations of the crystal point group that are either accidentally degenerate[10] or reflect a ''higher symmetry'' of the crystal[12] or of spin space.[9]

As briefly summarized below, experiments suggest an intriguing interplay between superconductivity and antiferromagnetism; however, an interpretation without significant ambiguity has not yet emerged. Here, we focus on one theoretical proposal: an odd-parity superconducting state with a two-dimensional order parameter that transforms like a single representation, the E_2 representation of the hexagonal symmetry group. This order parameter may also couple to the antiferromagnetic (AFM) order parameter. While the spatially homogeneous superconducting states of this model and their response to an applied magnetic field have been studied, there is comparatively little work that explores the effect of spatially inhomogeneous antiferromagnetism (SIAFM) on superconductivity. Motivated by recent work of Garg,[13] which concludes that spatially varying antiferromagnetism would rule out the two-dimensional representation models for UPt_3, we examine the sensitivity of an E_{2u} superconductor to SIAFM through numerical calculations of its response to two qualitatively different kinds of spatial configurations of the SIAFM. Since the free-energy functionals for an E_{2u} and an E_{1g} superconductor are formally identical, our results are also relevant to E_{1g} superconductors.

Antiferromagnetism is the prime suspect for inducing the zero-field double phase transition observed in specific-heat experiments on high-quality crystals. A coupling between AFM and superconducting order parameters is suggested by a downward kink in the magnitude of the modulus of the AFM order parameter at the superconducting transition.[2] In a comparison of specific-heat measurements with neutron-scattering experiments under pressure, Hayden *et al.*[3] observed that the disappearance of the double transition is correlated with the disappearance of signatures of antiferromagnetism. Recent work of Keizer *et al.*[14] further supports this correlation. Upon substituting Pd for Pt on a small number of sites, they find that the magnetic moment and the splitting of the double transition increase simultaneously with increasing Pd doping.

The nature of the antiferromagnetism is itself unusual. A signature of an AFM phase transition in thermodynamic, NMR (nuclear magnetic-resonance), and zero-field μSR (muon spin relaxation) experiments has so far not been observed.[15] This has been taken as evidence for the absence of long-range order and the existence of magnetic fluctuations on a characteristic scale smaller than neutron-scattering frequencies, but greater than those of NMR. This temporal fluctuation has largely been ignored and the antiferromagnetism has been taken to be static when considering the interaction of antiferromagnetism with superconductivity. While conventional thermodynamic signatures of the Néel temperature T_N have not been observed, more recent trans-

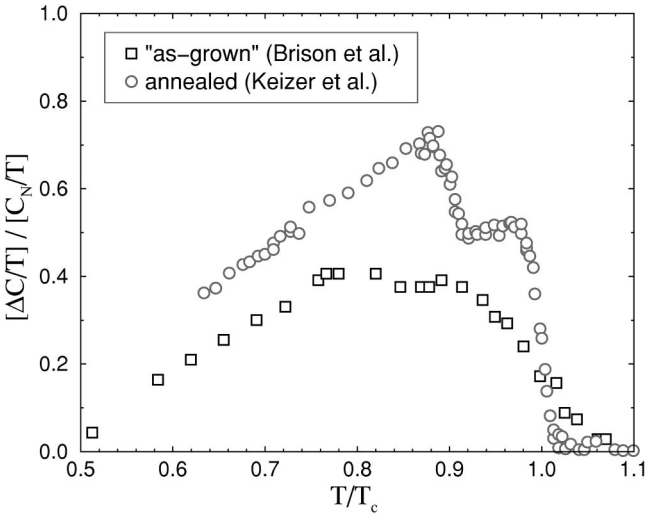

FIG. 1. Specific-heat data of a low-quality sample showing a single broad peak (Ref. 44) (squares) compared to that for a high-quality sample (Ref. 14). The latter reveals signatures of two closely spaced phase transitions. In the normal state $C_N/T \approx 430$ mJ/(K^2 mol).

verse high-field μSR experiments have detected anomalies at T_N as identified by neutron scattering.[16]

The appearance of the double transition was unexpected. As shown in Fig. 1, specific-heat experiments[17] prior to 1989 typically showed a single anomalously broad peak at the transition to superconductivity. An obvious explanation is that AFM domains increase in size during the annealing process, sharpening the distribution around two intrinsic superconducting transitions, but x-ray[2] and neutron-scattering[18] experiments fail to show any obvious correlation between domain size and annealing.

A commonly held physical picture is based on an interpretation of the neutron-scattering data. The AFM order with orthorhombic symmetry appears with $\sim 0.02\mu_B$ ordered moments constrained to lie in the basal plane. AFM order occurs in domains of uniform size ~ 30 nm that are randomly distributed over three **q** vectors that are oriented at 0°, 120°, and 240° with respect to the **a*** axis. The moments are essentially rigidly locked to the lattice for fields in excess of the zero-temperature upper critical field of the superconducting state.[19,20]

This picture is not firmly established. Existing neutron-scattering data are unable to rule out the possibility that instead of domains of a single-**q** structure, AFM order appears in a triple-**q** structure that preserves the symmetry of the crystal lattice.[20] Moreover, a recent careful analysis of the neutron-scattering data[21] finds that no conclusion can be drawn from existing data on whether the staggered moment remains fixed to the lattice or whether it rotates with an applied magnetic field. Existing data also cannot distinguish randomly oriented abutting domains with small magnetic moments from small domains with magnetic moments of $\sim 1\mu_B$ interspersed in an otherwise nonmagnetic system.

Whether antiferromagnetism occurs in a few large domains with staggered moments that are free to rotate in an applied field, or whether it is strongly spatially varying with staggered moments that are rigidly fixed to the lattice, is important in determining the symmetry of the superconducting states, particularly for states near the upper transition temperature. Several authors take the view that this quasistatic antiferromagnetism acts as a symmetry-breaking field (SBF) and lifts the degeneracy among components of a multicomponent order parameter resulting in two superconducting phase transitions separated by ~ 50 mK that are observed in zero field.[8,22–24,9,25–30] A two-component odd-parity order parameter that transforms like the two-dimensional E_{2u} representation of the hexagonal symmetry group D_{6h} is one of the more promising proposals.[7,31] At low temperature or in the absence of the SBF, weak-coupling BCS theory shows that the homogeneous equilibrium state breaks time-reversal symmetry. Further calculations using weak-coupling BCS theory show that thermal conductivity,[32] transverse sound attenuation,[33] and upper critical fields[34] of this state are in good agreement with experiments for temperatures in the low-temperature phase.[35] Coupling to a SBF has been included within a Ginzburg-Landau (GL) theory developed for a single-domain superconducting state. Signatures of a double phase transition are apparent in the specific heat and lower critical field,[23,7] and in the cores of vortices.[36] In contrast to two-dimensional even-parity E_{1g} and E_{2g}, and to odd-parity E_{1u} order parameters, the E_{2u} model can allow for a tetracritical point for arbitrary field orientations in the H-T phase diagram. An enhancement of this model includes the competition between magnetic anisotropy and Zeeman energies of the magnetic order parameter,[37] and reproduces the angular dependence of the upper critical field observed in experiment.[38]

Within the E_{2u} model, comparatively little has been done to explore the effect of coupling superconductivity and spatially inhomogeneous antiferromagnetism. Motivated by the quenched domain interpretation of the neutron-scattering data, early work on E-representation superconductivity by Joynt *et al.*[25] and by Mineev[39] focused on abutting AFM domains that are uniform in size with dimensions of a superconducting coherence length and considers the possibility of a superconducting glass phase. Based on a variational calculation for domains of uniform size and on calculations for a one-dimensional ''toy model,'' Garg[13] argued that the pure E-representation models are ''incompatible'' with UPt_3 for the small domains suggested by the neutron-scattering experiments.

Taking the AFM order to be static, we explore the sensitivity of E_{2u} superconductivity to spatially varying AFM order in two models for the (disordered) domain structure of the AFM state: Model I, abutting AFM domains of uniform size with orientations that are equally distributed over the allowed **q** vectors; and Model II, small domains interspersed in a homogeneous AFM background. We consider these models to represent limiting cases for the configuration of the SIAFM. The first model corresponds to the standard interpretation of the neutron-scattering data. The second model begins with uniform AFM order and adds ''nanodomains'' with random position and orientation of the staggered magnetization; this provides the broadening mechanism for the linewidth of neutron-scattering data. We present numerical

solutions of the GL equations in two spatial dimensions and focus on contributions to the free energy, the specific heat, and the nature of the superconducting state. Our results for Model I agree with those for Garg's simple periodic model. While neither model provides an adequate account of experiment, our results for Models I and II differ, and taken together they *do not* lead to Garg's conclusion that the E_{2u} model is incompatible with UPt_3. Rather, they suggest that a reasonably accurate model of the spatial dependence of the antiferromagnetism is required to make meaningful comparisons with experiment. In a forthcoming work, we discuss other domain configurations along with the effects of dimensionality and the possible role of superconducting glass phases.[40] Central results of this paper are contained in the comparison of specific-heat calculations with experiment for both models.

In Model I, the signatures of the superconducting transitions rapidly smear and broaden with decreasing domain size. The SBF introduces a convenient length scale ξ_ε (defined below) that, for UPt_3, is some three times larger than the zero-temperature superconducting coherence length. For domain sizes of $10\xi_\varepsilon - 20\xi_\varepsilon$, the calculated specific heat compares well with data from experiment.[14] This homogeneous domain size model does not agree with neutron-scattering experiments that, when viewed through the lens of Model I, would suggest a much smaller domain size $\sim 1\xi_\varepsilon - 3\xi_\varepsilon$. As the domain size is decreased below $\sim 2\xi_\varepsilon$, only a single superconducting transition appears in the specific heat. While the suppression of the double transition with decreasing domain size suggests an obvious explanation for the appearance of the double transition upon annealing of as-grown samples (see Fig. 1), this explanation appears to be inconsistent with magnetic x-ray and neutron-scattering data that are interpreted as showing no change in domain size with annealing.

In contrast, Model II is not as sensitive to the density of nanodomains. Specific-heat signatures remain sharp even for a high density of ''nanodomains'' and resemble those for high-quality crystals. Although these signatures remain sharp, for coverages larger than $\sim 75\%$ only a single superconducting transition occurs.

While neither model provides an adequate account of the experimental data, the calculations presented here demonstrate the sensitivity of E_{2u} superconductivity to SIAFM and suggest that a reasonably accurate description of the spatial variation of the underlying antiferromagnetism is crucial in drawing conclusions about the symmetry of the superconducting states.

II. COUPLED SUPERCONDUCTIVITY AND ANTIFERROMAGNETISM

A. The *E*-representation model

We begin by reviewing the Ginzburg-Landau free energy for an E_{2u} superconductor coupled to a SBF. We take the E_{2u} gap matrix $\Delta_{\alpha\beta}(\mathbf{k},\mathbf{r})$ to be the superconducting order parameter; it has the form

$$\Delta_{\alpha\beta}(\mathbf{p}_f,\mathbf{r}) = \mathbf{e}(\mathbf{p}_f)\cdot\boldsymbol{\eta}(\mathbf{r})(\hat{c}\cdot i\vec{\sigma}\sigma_y)_{\alpha\beta}, \tag{1}$$

where $\mathbf{e}(\mathbf{p}_f)=[e_1(\mathbf{p}_f),e_2(\mathbf{p}_f)]$ are basis functions on the Fermi surface that transform among each other under the operations of the D_{6h} symmetry group, $\boldsymbol{\eta}(\mathbf{r}) = [\eta_1(\mathbf{r}),\eta_2(\mathbf{r})]$ are Cooper-pair amplitudes that are functions of the Cooper-pair center of mass $\mathbf{r}$, $\hat{c}$ is a unit vector along the c axis of the crystal, and σ_i are Pauli matrices in spin space. Explicit expressions for E_{2u} and other basis functions may be found in Refs. 7,8, and 32. The GL free-energy density is

$$f(\mathbf{r}) = f_{\text{bulk}}(\mathbf{r}) + f_{\text{grad}}(\mathbf{r}) + f_{\text{field}}(\mathbf{r}). \tag{2}$$

Symmetry constrains the form of the bulk, gradient, and field contributions for an E_{2u} superconductor to be[7]

$$f_{\text{bulk}} = \alpha(T)|\boldsymbol{\eta}|^2 + \beta_1|\boldsymbol{\eta}|^4 + \beta_2|\boldsymbol{\eta}\cdot\boldsymbol{\eta}|^2, \tag{3}$$

$$f_{\text{grad}} = \kappa_1(D_i\eta_j)(D_i\eta_j)^* + \kappa_2(D_i\eta_i)(D_j\eta_j)^* + \kappa_3(D_i\eta_j)(D_j\eta_i)^* + \kappa_4(D_z\eta_j)(D_z\eta_j)^*, \tag{4}$$

$$f_{\text{field}} = \frac{1}{8\pi}|\mathbf{b}|^2, \tag{5}$$

where $\alpha(T)=\alpha_0(T-T_0)$, α_0 is a constant, T_0 is the transition temperature, $\mathbf{b}=\boldsymbol{\partial}\times\mathbf{A}$ is the magnetic field, and $D_j = \partial_j - i(2e/\hbar c)A_j$ is the gauge-invariant gradient. In the calculations that follow for a spatially varying SBF, we restrict ourselves to two dimensions and κ_4 plays no role. In weak-coupling BCS theory for an E_{2u} order parameter, the parameters κ_2 and κ_3 are small for Fermi surfaces with axial symmetry;[7] we take $\kappa_2=\kappa_3=0$ and write $\kappa\equiv\kappa_1$ for notational convenience. Weak-coupling BCS theory also predicts that $\beta_2=\beta_1/2$ independent of the shape of the Fermi surface and that the homogeneous equilibrium order parameter that minimizes the free energy is doubly degenerate, breaks time-reversal symmetry, and is of the form $\boldsymbol{\eta}\sim(1,\pm i)$.

The orientation of the AFM order parameter $\mathbf{N}(\mathbf{r})$ may fluctuate dynamically. An estimate of the magnetic fluctuation time τ_{mag} from the energy-resolution limited magnetic Bragg peaks obtained from elastic neutron-scattering experiments gives $\tau_{\text{mag}}\sim 500$ ps.[41] Because this fluctuation time is slow compared to the characteristic time scale of the superconducting state $\tau_{sc}\sim h/\Delta_0\sim 50$ ps, we take the SBF to arise from static AFM order[25] and calculate equilibrium solutions of the GL functional in the presence of spatially varying AFM order.

The transition temperature below which antiferromagnetic order occurs is an order of magnitude larger than the superconducting transition. In a mean-field description of the AFM order, the order parameter is well developed at the transition to superconductivity. Below the superconducting transition, the neutron-scattering data suggests that the modulus of the staggered magnetization decreases. Over the temperature range for which a GL theory of superconductivity is valid, the modulus of the staggered magnetization changes by less than 5%. Since this change is small, we take the staggered magnetization to be a fixed external field and neglect the effect of superconductivity on antiferromagnetic order.[42] The leading contribution to the free energy from the

coupling of antiferromagnetism and superconductivity is second order in $\boldsymbol{\eta}$ and of the form

$$f_{\rm sbf} = 2\varepsilon\alpha_0(|\mathbf{N}\cdot\boldsymbol{\eta}|^2 - \tfrac{1}{2}|\boldsymbol{\eta}|^2) = \varepsilon\alpha_0\boldsymbol{\eta}^\dagger\begin{pmatrix} -\cos 2\theta & \sin 2\theta \\ \sin 2\theta & \cos 2\theta \end{pmatrix}\boldsymbol{\eta}, \quad (6)$$

where $\mathbf{N}=[\sin\theta(\mathbf{r}),\cos\theta(\mathbf{r})]$ is a normalized direction vector of the staggered magnetization, and ε is a coupling constant proportional to the square of the staggered magnetization. Symmetry also allows a coupling of the SBF to the gradient in the E_{2u} model,[7,43] so that $f_{\rm grad}$ is given by

$$f_{\rm grad} = \kappa_1^+|D_i\eta_1|^2 + \kappa_1^-|D_i\eta_2|^2 \quad (7)$$

with

$$\kappa_1^\pm = \kappa_1(1\pm\varepsilon_\perp\mathbf{N}^2). \quad (8)$$

This term, together with the $\hat{c}$-axis gradient terms, determines the kink and possible tetracritical point on the upper critical-field curve. Because the magnitude of the gradient coupling to the SBF is small, being of the order $\varepsilon_\perp\sim\varepsilon\sim\Delta T_c/T_c$, it will not significantly affect our results, and so we neglect the (direct) coupling of $\mathbf{N}$ to $\boldsymbol{\eta}$ through the gradient terms for the calculation of thermodynamic properties in zero magnetic field.

The symmetry-breaking term in Eq. (6) is combined with Eq. (2) to give the free-energy density

$$f = \alpha_-(T)|\eta_1|^2 + \alpha_+(T)|\eta_2|^2 + \varepsilon\alpha_0\sin 2\theta(\eta_1\eta_2^* + c.c.) + \beta_1(|\eta_1|^2+|\eta_2|^2)^2 + \beta_2|\eta_1^2+\eta_2^2|^2 + \kappa(D_i\eta_j)(D_i\eta_j)^* + \frac{1}{8\pi}\mathbf{b}^2, \quad (9)$$

with $\alpha_\pm(T)=\alpha(T)\pm\varepsilon\alpha_0\cos 2\theta$. For temperatures very near the normal-superconducting transition, the second-order terms that include the coupling to the SBF dominate and ''real'' phases of the form $\boldsymbol{\eta}\sim(\cos\theta,\sin\theta)e^{i\varphi}$ minimize the free energy.

B. Single AFM Domain and Estimation of GL Parameters

Without loss of generality, the salient features of coupling to uniform antiferromagnetism (single infinite domain) can be seen by taking $\mathbf{N}(\mathbf{r})=(0,1)$ and the coupling to the SBF to be positive, $\varepsilon>0$, so that $f_{\rm sbf}$ favors $\boldsymbol{\eta}\perp\mathbf{N}$. At the temperature $T_{c+}^{\rm hom}=T_0+\varepsilon$, a phase transition occurs from the normal state to a spatially homogeneous superconducting phase $\boldsymbol{\eta}\propto(1,0)$. At a lower temperature $T_{c-}^{\rm hom}=T_0-\varepsilon/\beta$, there is a second phase transition to a time-reversal symmetry-breaking phase $\boldsymbol{\eta}\propto[1,\pm ir(T)]$, where $\beta=\beta_2/\beta_1$ and $r(T)$ is a function that grows rapidly and smoothly from 0–1 as T is lowered.[23]

The specific-heat jumps (per volume) at the two phase transitions $T_{c+}^{\rm hom}$ and $T_{c-}^{\rm hom}$, measured relative to the normal state, are calculated from a derivative of the free energy and are given by[23]

$$\triangle C_+^{\rm hom} = T_{c+}^{\rm hom}\alpha_0^2/2\beta_{12}, \quad (10)$$

$$\triangle C_-^{\rm hom} = T_{c-}^{\rm hom}\alpha_0^2/2\beta_1, \quad (11)$$

with $\beta_{12}=\beta_1+\beta_2$. The ratio of the heat-capacity jumps is

$$\frac{\triangle C_-^{\rm hom}}{\triangle C_+^{\rm hom}} = \frac{T_{c-}^{\rm hom}}{T_+^{\rm hom}}(1+\beta). \quad (12)$$

Using these equations and the specific-heat data, we estimate the ratio $\beta\approx 0.42-0.65$.[44,14] Noting that the weak-coupling value of β lies comfortably in this range, we take $\beta=1/2$ in the calculations below. Further, the measured $\hat{c}$-axis H_{c2} slopes[4,5] of ~ 6.6 T/K imply within a coarse-grained analysis that $\kappa/\alpha_0\approx 50$ K nm^2, i.e., a zero-temperature GL coherence length $\xi_0=\sqrt{\kappa/(\alpha_0 T_{c+}^{\rm hom})}\approx 10$ nm. This estimate of ξ_0 in the basal plane is in very good agreement with other reports.[45]

III. SPATIALLY INHOMOGENEOUS ANTIFERROMAGNETISM

We now consider the possibility that the orientation of $\mathbf{N}$ varies in the crystal lattice $\mathbf{N}=\mathbf{N}(\mathbf{r})$ and explicitly investigate two cases: (1) abutting antiferromagnetic domains of uniform size $\xi_{\rm afm}$ with orientations distributed equally among the three possible $\mathbf{q}$ vectors, and (2) randomly dispersed ''nanodomains'' with characteristic dimensions of order the superconducting coherence length. For SIAFM, an analytic solution is generally no longer possible and it is necessary to solve the GL equations numerically. The resulting superconducting state will be complicated, because of the competition between the condensation energy gained by $\boldsymbol{\eta}$ orienting in directions preferred by the SBF and the gradient energy cost to twist the orientation of the order parameter from domain to domain. The response of an E_{2u} superconductor to these two models for SIAFM differs as described below.

A. Preliminaries

For numerical calculation, it is convenient to introduce a scaled order parameter $\tilde{\boldsymbol{\eta}}=\boldsymbol{\eta}/\eta_0$, where η_0 is the modulus of the real phase solution of a homogeneous single domain $\eta_0=\sqrt{\alpha_0\varepsilon t/2\beta_{12}}$ that appears in the presence of uniform AFM order at a transition temperature $T_{c+}^{\rm hom}=T_0+\varepsilon$. All temperatures are given in terms of a reduced temperature $t=(T_{c+}^{\rm hom}-T)/\varepsilon$. Scaling Eq. (9) to the magnitude of the free-energy density of the homogeneous single-domain solution in the high-temperature phase $|f_0(t)|=(\alpha_0\varepsilon t)^2/(4\beta_{12})$, a dimensionless Ginzburg-Landau free-energy density $\tilde{f}$ is obtained, which is of the form

$$\tilde{f} = -2\Big[(1-\tau\sin^2\theta)|\tilde{\eta}_1|^2 + (1-\tau\cos^2\theta)|\tilde{\eta}_2|^2 - \tau\sin 2\theta\,\mathrm{Re}\,\tilde{\eta}_1\tilde{\eta}_2^* - \frac{1}{2}|\tilde{\boldsymbol{\eta}}|^4 + \frac{2\beta}{1+\beta}|\tfrac{1}{2}\tilde{\boldsymbol{\eta}}\times\tilde{\boldsymbol{\eta}}^*|^2\Big] + \tau(|\tilde{D}_i\tilde{\eta}_1|^2 + |\tilde{D}_i\tilde{\eta}_2|^2), \tag{13}$$

where all lengths are measured in terms of the SBF length $\xi_\varepsilon = \sqrt{\kappa/\alpha_0\varepsilon}$, $\tilde{D}_i = \xi_\varepsilon D_i$, and $\tau = 2/t$.

For ease of calculation, we take a square computational mesh with a step size $\triangle x = \triangle y = 0.2\xi_\varepsilon$. We tested our GL simulations on triangular lattices, which are more natural given the apparent hexagonal crystal symmetry of UPt_3, and have found no qualitative differences for averaged quantities. Periodic boundary conditions were imposed. We take the GL parameters to be $\beta = 1/2$ and $\kappa = \alpha_0\varepsilon\xi_\varepsilon^2$.

As the superconducting order parameter twists to accommodate the spatially inhomogeneous symmetry-breaking field, time-reversal symmetry-breaking phases may appear in localized regions even for temperatures near the normal-superconducting phase boundary, where ''real'' phases are expected to dominate. To detect the appearance of these phases, we calculate

$$\mathbf{M}_{\rm orb}(\mathbf{r}) = \frac{1}{2i}\tilde{\boldsymbol{\eta}}(\mathbf{r})\times\tilde{\boldsymbol{\eta}}(\mathbf{r})^*, \tag{14}$$

which is (apart from a factor dependent on the gradient terms[7]) the spontaneous magnetization that arises from the internal orbital motion of a Cooper pair. Note that $\mathbf{M}_{\rm orb}$ is a real vector constrained by symmetry to point along $\pm\hat{c}$. For a homogeneous single domain, $\mathbf{M}_{\rm orb}$ vanishes between the two transitions, as it must for a ''real'' phase. At the lower transition, the second component of the order parameter begins to grow with a phase relative to the first and $\mathbf{M}_{\rm orb}$ increases rapidly with decreasing temperature signaling broken time-reversal symmetry. As expected, the temperature dependence of $\mathbf{M}_{\rm orb}$ is consistent with a second-order phase transition in mean-field theory $|\mathbf{M}_{\rm orb}(T)| \sim \sqrt{T_{c-}^{\rm hom} - T}$, for $T \leqslant T_{c-}^{\rm hom}$.

The calculation of free energies and spatially averaged quantities involves a summation over the lattice. We adopt the notation

$$\langle A(\mathbf{r})\rangle_{\mathbf{r}} = N^{-2}\sum_{i=1}^{N}\sum_{j=1}^{N} A(x_i, y_j), \tag{15}$$

where N^2 is the number of computational mesh points and the position vector $\mathbf{r} = (x,y)$. In this notation, the spatially averaged orbital moment is $\langle\mathbf{M}_{\rm orb}(\mathbf{r})\rangle_{\mathbf{r}}$. In the case of Model I, we solved for several antiferromagnetically ordered domain sizes on a square lattice. For Model II we have found solutions of the GL equations for different sets of random configurations of the SBF and have not found any discernible differences for spatially averaged quantities. We attribute this ''self-averaging'' of the quenched disorder of the randomized SBF to our relatively large system size (this would be exact for an infinite system) and to the large concentration of nanoscale defects (9%–79%).

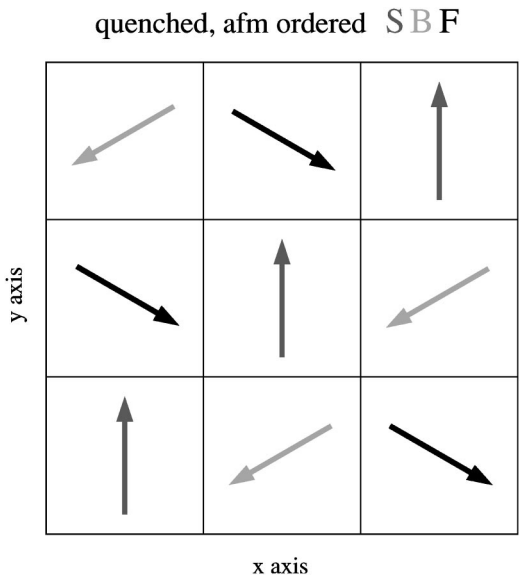

FIG. 2. Structure of AFM domains assumed in Model I. For convenience, a computational mesh with a square geometry was chosen; explicit comparison with calculations on triangular meshes do not change our central conclusions.

B. Model I—Checkerboard

The spatially varying staggered moment configuration consists of abutting domains as shown in Fig. 2. The orientation pattern of $\mathbf{N}(\mathbf{r})$ was generated so that nearest-neighbor domains do not have a SBF of the same orientation and so that there is no net staggered magnetization. The influence of the SBF is greatest at high temperature and the nature of the superconducting phase depends on the size of the AFM domains relative to the superconducting coherence length. At sufficiently low temperature, the order parameter is $\boldsymbol{\eta}(\mathbf{r}) \propto (1,i)$ to an excellent approximation; for most purposes the coupling to the SBF leads to a negligible correction to the order parameter.

The effect of domain size on the superconducting transitions is apparent in Fig. 3. For large domains, two reasonably sharp transitions are apparent. They smear rapidly as the domain size is decreased until for $\xi_{\rm afm} \sim 2\xi_\varepsilon$ only one transition appears for the size of our computational mesh together with imposed periodic boundary conditions. A comparison of the numerical calculations of Fig. 3 for our model in two dimensions with the specific-heat calculations for Garg's one-dimensional model presented in Fig. 2 of Ref. 13 shows that these are in good agreement given the simplicity of the ''toy'' model.[46]

The lower panel of Fig. 3 shows the temperature dependence of the spatially averaged spontaneous magnetization that reflects the nature of the two phase transitions. For an infinitely large single domain, $\langle\mathbf{M}_{\rm orb}(\mathbf{r})\rangle_{\mathbf{r}}$ vanishes in the high-temperature phase where the order parameter is ''real'' and rapidly increases below the lower phase transition $T_{c-}^{\rm hom}$, as described above. As the domain size decreases, $\langle\mathbf{M}_{\rm orb}(\mathbf{r})\rangle_{\mathbf{r}}$

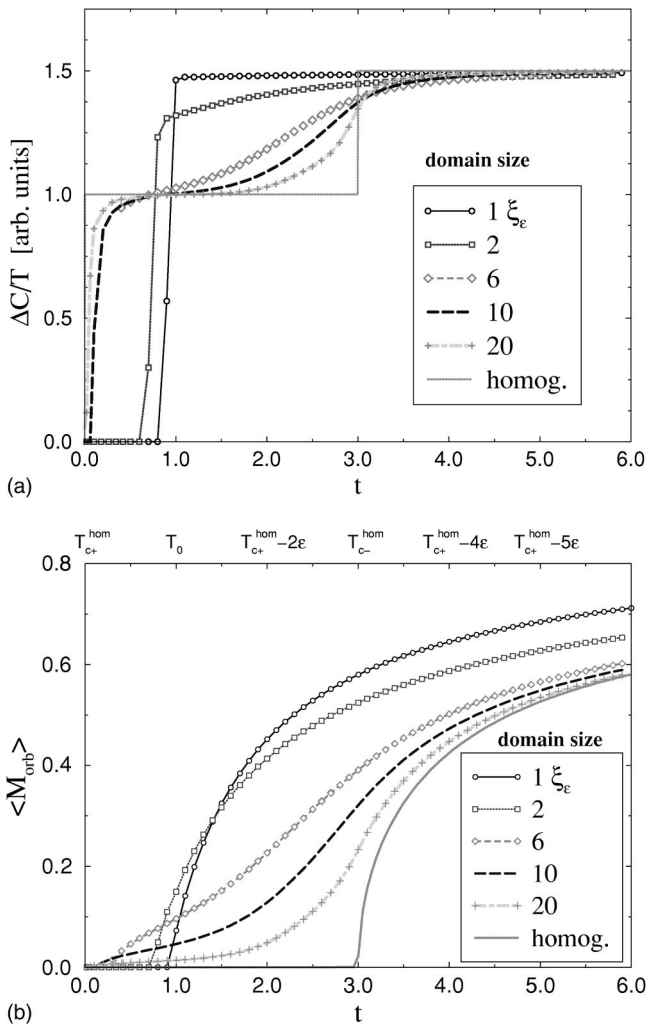

FIG. 3. Top: The specific heat for Model I in units of the upper specific-heat jump of the spatially homogeneous system $\triangle C_+^{\rm hom}/T_{c+}^{\rm hom}$ for various AFM domain sizes measured in units of the SBF length ξ_ε. The temperature t is measured relative to the upper superconducting transition and *decreases* in the positive x direction $t=(T_{c+}^{\rm hom}-T)/\varepsilon$. Bottom: The corresponding spatially averaged spontaneous magnetization $\langle \mathbf{M}_{orb}(\mathbf{r})\rangle_{\mathbf{r}}$ as a function of t and for the same domain sizes.

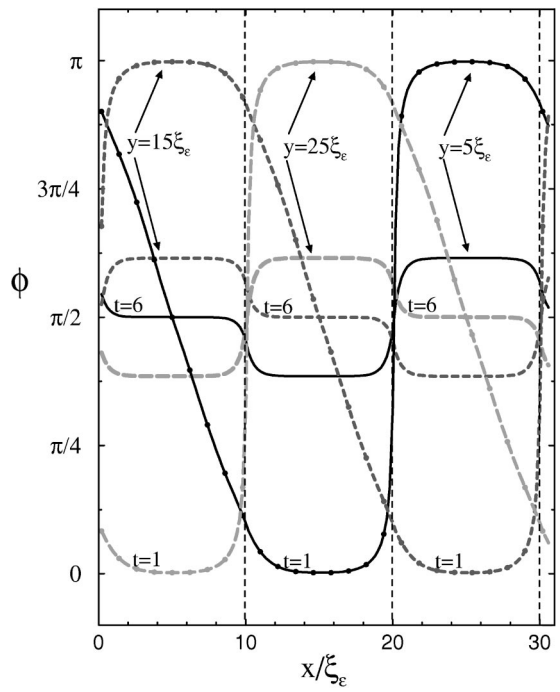

FIG. 4. Spatial cuts of the relative angle ϕ between the order parameters η_1 and η_2 along the x axis for a fixed y coordinate at temperatures $t=1$ and $t=6$. The AFM domain size is $10\xi_\varepsilon$ and $\phi=\angle(\eta_1,\eta_2)$. The same parameters are used in Fig. 5. A relative angle of $\phi=\pi/2$ signals a superconducting phase that breaks time-reversal symmetry. The low-temperature phase ($t=6$) breaks time-reversal symmetry on average, while the high-temperature phase ($t=1$) breaks time-reversal symmetry predominantly in the domain walls (indicated as vertical dashed lines).

becomes finite but remains small for temperatures below T_{c+} and above $T_{c-}^{\rm hom}$. The time-reversal symmetry-breaking phase appears with increasing strength as the order parameter tries to twist from domain to domain. For the largest domains, the specific heat shows two phase transitions (albeit rounded by spatial fluctuations), even though $\langle \mathbf{M}_{\rm orb}(\mathbf{r})\rangle_{\mathbf{r}}$ is finite between the two transitions. For the smallest domain sizes only one transition is apparent[47] with an onset approximately that of the transition temperature in the absence of coupling to the SBF, T_0.

The twisting and flapping of the two superconducting order parameters η_1 and η_2 across the domain walls is apparent in the plots of the relative phase angle ϕ between η_1 and η_2 in Figs. 4 and 5. The flapping or unwinding of the relative phase in Fig. 4 follows the antiferromagnetism on average, producing reasonable narrow (order $\sim\xi_\varepsilon$) superconducting domain walls in registry with the AFM domain walls. Occasionally, the relative phase unwinds from $0-\pi$ over an entire domain. Fig. 5 shows the spatially varying superconducting order parameter for the particular AFM configuration shown in Fig. 2 and a domain size of $10\xi_\varepsilon$. The spatial variation of the modulus of $\boldsymbol{\eta}$ shown at low and at high temperature in Figs. 5(a) and (b), tracks the underlying AFM domain structure. As expected, at high temperature, there is a suppression of superconductivity at the domain walls. At low temperature, there is a small reduction in the component of $\boldsymbol{\eta}$ parallel to $\mathbf{N}$ in the $\sim(1,i)$ phase preferred by the fourth-order terms in the free energy and a negligibly small suppression of superconductivity occurs in the *center* of the domain. At high temperature, the components of the superconducting order parameter are ''real'' in the interior of the domains. The orientation of the order parameter attempts to follow the AFM order on average. The orientation of $\boldsymbol{\eta}$ does not follow that of $\mathbf{N}$ perfectly. A side-by-side comparison of Figs. 5(d) and 2 shows that even for these relatively large domains, the different orientation of the SBF in adjacent domains forces a compromise in the orientation of $\boldsymbol{\eta}$ as it twists from domain to domain. For example, $\boldsymbol{\eta}$ makes a 45° angle with respect to the SBF at the center of the domain $(0-10,0-10)$ in Fig. 5(d). For temperatures below the second phase transition, the superconducting phase is essentially $(1,i)$ with a small perturbation from the AFM order. This is evident from Figs. 4

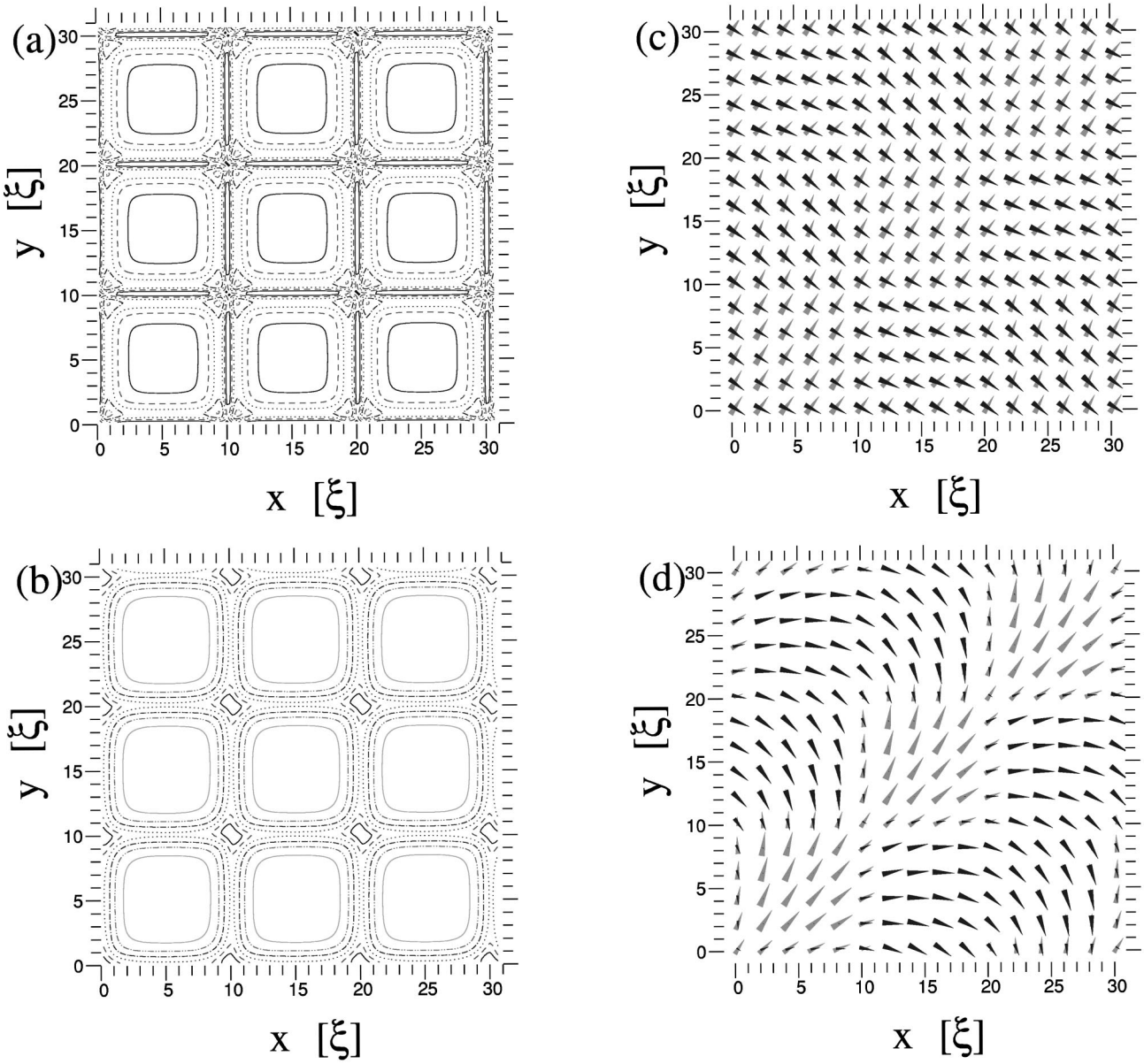

FIG. 5. Domain structure of the Model I superconducting state induced by the coupling to homogeneous AFM domains of size $10\xi_\varepsilon \times 10\xi_\varepsilon$ with three equivalent orientations $0°, \pm 120°$ of the SBF. Distances are in units of ξ_ε. (a): Contour plot of $|\boldsymbol{\eta}(\mathbf{r})|/\langle|\boldsymbol{\eta}(\mathbf{r})|\rangle_\mathbf{r}$ at steps 0.999 (solid), 1.000 (dash), 1.001 (dot), 1.002 (dash dot), and 1.003 (dash dot dot) at temperature $t=6$. $|\boldsymbol{\eta}|$ is minimum in the domain center. (b): Contour plot of $|\boldsymbol{\eta}(\mathbf{r})|/\langle|\boldsymbol{\eta}(\mathbf{r})|\rangle_\mathbf{r}$ at steps 0.80 (solid), 0.85 (dash), 0.90 (dot), 0.95 (dash dot), 1.00 (dash dot dot), and 1.05 (light solid) at temperature $t=1$. $|\boldsymbol{\eta}|$ is maximum in the domain center. (c) and (d): The complex order parameter components η_1 (light) and η_2 (dark) are plotted as two-dimensional vectors, where the relative size of the vector is proportional to its magnitude. In the low-temperature phase $t=6$ in (c), $\eta_1 \perp \eta_2$ on average, while in the high-temperature phase in (d), $\eta_1 \| \eta_2$ almost always. The orientation of the SBF is the same as in Fig. 2.

and 5(c), which show a sizeable phase angle $\sim \pi/2$ between the η_1 and η_2 components. At high temperature, the order parameter is mildly suppressed at the domain walls where the relative phase angle between the η_1 and η_2 components is sizeable, reaching $\sim \pi/2$ at the corners, indicative of the appearance of time-reversal symmetry-breaking phases in the domain walls.

For various domain sizes, the nature of the spatially inhomogeneous superconducting state is reflected in the ratio $\langle f_{\rm sbf}(\mathbf{r})\rangle_\mathbf{r}/\langle f_{\rm grad}(\mathbf{r})\rangle_\mathbf{r}$, where $\langle f_{\rm sbf}(\mathbf{r})\rangle_\mathbf{r}$ measures, in an average way, the extent to which the superconducting order parameter tracks the twisting of the SBF, and $\langle f_{\rm grad}(\mathbf{r})\rangle_\mathbf{r}$ measures the energy cost of twisting the order parameter. The ratio $\langle f_{\rm sbf}(\mathbf{r})\rangle_\mathbf{r}/\langle f_{\rm grad}(\mathbf{r})\rangle_\mathbf{r}$ plotted in Fig. 6 is largely temperature independent and insensitive to domain size near T_{c+}, i.e., $t\to 0$ for large domains. For the smallest domain size, the ratio is significantly larger owing mostly to a smaller $\langle f_{\rm grad}(\mathbf{r})\rangle_\mathbf{r}$ and the stiffness of the condensate. This suggests the appearance of a qualitatively different phase—a strongly disordered superconducting phase.[48] As can be seen

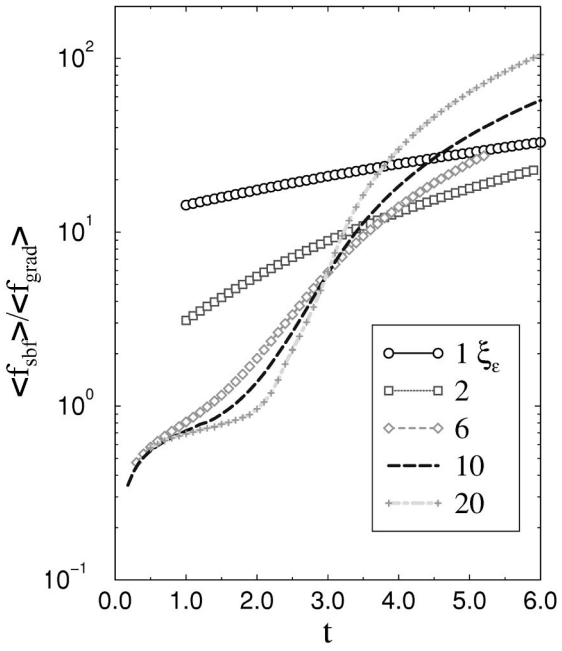

FIG. 6. The ratio of the contributions to the free energy from the SBF coupling term and the gradient term $\langle f_{\rm sbf}(\mathbf{r})\rangle_{\mathbf{r}}/\langle f_{\rm grad}(\mathbf{r})\rangle_{\mathbf{r}}$ for Model I and for various domain sizes. Note that for the smallest domains the ratio is significantly larger at high temperatures $t<3$, reflecting a new (strongly disordered) state in which the twisting of the order parameter decouples from the AFM order and on average $\langle \boldsymbol{\eta}(\mathbf{r})\rangle_{\mathbf{r}} \sim (1,i)$.

from Fig. 3, near T_{c+} this phase differs from that for larger domains, because time-reversal symmetry is broken globally and not just in the spatially restricted regions between superconducting domains.

Since GL theory does not predict the proper temperature dependence of the specific heat, we apply a correction to recover the correct temperature dependence near the double transitions so that GL results may be compared with experiment. We compute the specific heat self-consistently within weak-coupling BCS theory for a homogeneous single AFM domain for different sets of T_c splittings in the clean limit and compare it with the GL result. A reasonable approximation to the BCS theory temperature dependence for a small temperature range below the normal-superconducting phase transition can be obtained by multiplying the homogeneous GL result by a factor proportional to εt, as shown in Fig. 7.

Our results are shown together with specific-heat experiments in Fig. 8. For ease of comparison, the experimental results have been scaled so that the peak in the specific heat at the lower phase transition agrees with the corresponding feature for a homogeneous SBF. Calculations for domain sizes $\sim 6\xi_\varepsilon - 20\xi_\varepsilon$ show two phase transitions that are blurred by the spatial inhomogeneity of the magnetic order in a way that resembles experiments. From the comparison, we deduce that the coupling to the symmetry-breaking field is small, $\varepsilon \approx 18$ mK, compared to $T_{c+} \approx 540$ mK.

The domain sizes consistent with specific-heat experiments, $10\xi_\varepsilon - 20\xi_\varepsilon$ ($\sim 30\xi_0 - 60\xi_0$), are much larger than the uniformly sized $1\xi_\varepsilon - 2\xi_\varepsilon$ ($\sim 3\xi_0 - 6\xi_0$) domains attributed to neutron-scattering experiments. For the latter small

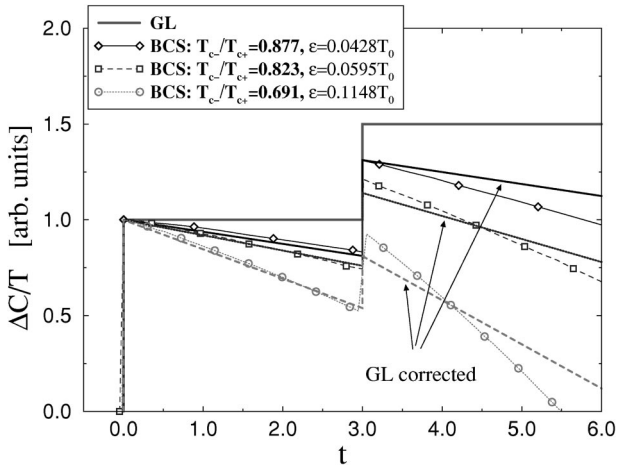

FIG. 7. The specific heat for an E_{2u} superconductor computed from weak-coupling BCS theory for various SBF coupling strengths ε (symbols), and from GL theory for a single AFM domain. The BCS-theory temperature dependence can be approximately recovered from the GL-theory specific heat using a multiplicative factor that is linear in $t\varepsilon$.

domains, only a single phase transition would appear in these calculations. This reflects the relative stiffness of the superconducting order parameter as compared to the condensation energy gained from orienting the superconducting order parameter in a direction favorable to the local AFM order parameter.

C. Model II—''Swiss Cheese''

The superconducting state of Model I is very sensitive to the size of the AFM domains. To explore the response of an E_{2u} superconductor to different spatial AFM configurations,

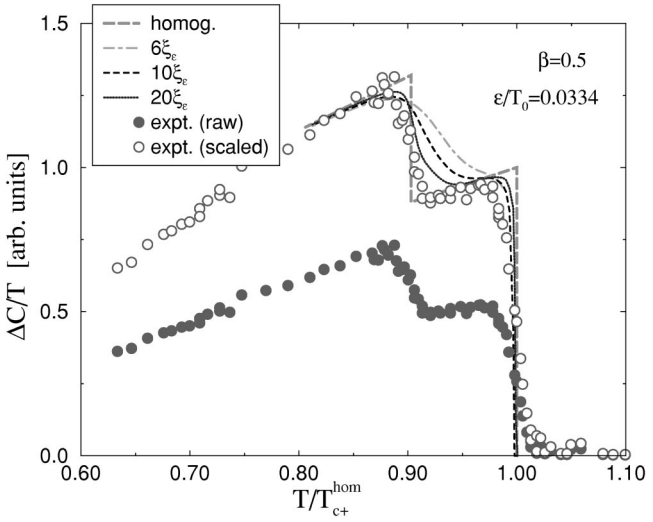

FIG. 8. Calculated specific heat for Model I for a single domain and for various domain sizes in comparison with experiment (filled circles) normalized by C_N/T (Ref. 14). For ease of comparison, the experimental data scaled by a numerical factor (open circles) are also presented. The T dependence of the GL results has been corrected according to Fig. 7.

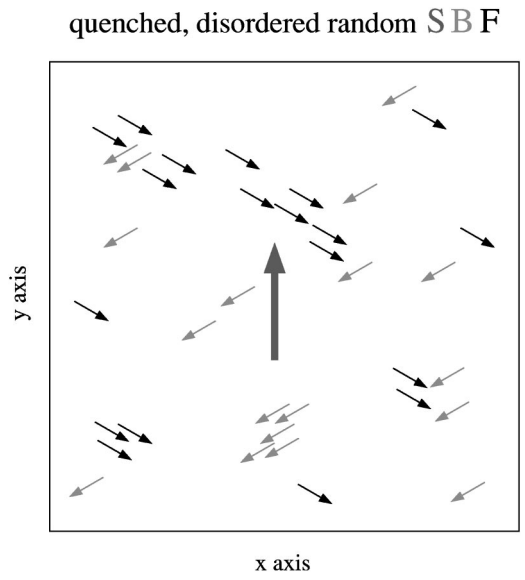

FIG. 9. The spatial orientation of the SBF for the randomly dispersed nanodomains (small arrows) in the presence of a uniform SBF in the background (big arrow) of Model II.

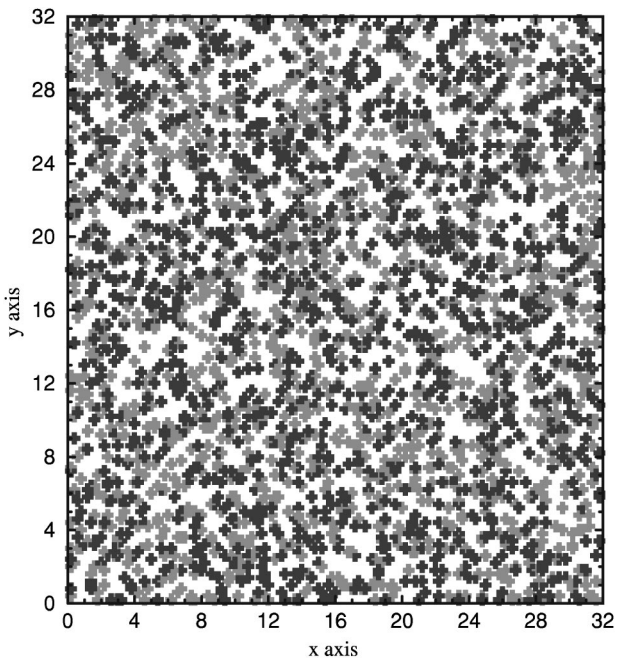

FIG. 10. A typical spatial distribution of cross-shaped nanodomains (nanodefects) covering approximately 44% of the $32\xi_\varepsilon \times 32\xi_\varepsilon$ numerical mesh in the presence of a uniform AFM background.

we consider a model that represents what might be viewed as an opposite extreme from the abutting uniformly sized domains of Model I. In Model II, nanoscale-sized AFM domains permeate a large single (''infinite'') AFM domain like the holes in Swiss cheese. This picture is motivated by the observation of *intrinsic* defects (most likely dislocation lines or stacking faults) in high-quality and high-purity UPt_3 samples[49–51] and by the observation that neutron-scattering data cannot distinguish between the commonly accepted picture of abutting uniform domains with small moments and small domains with significantly larger moments. These *intrinsic* defects may act as nucleation centers for the random-field-like symmetry-breaking field, ''nanodomains,'' and may provide a natural explanation for the linewidth broadening of the AFM Bragg peak in reciprocal space as seen in neutron-diffraction measurements.[1]

We used a standard pseudorandom number generator to uniformly distribute the nanodomains on our computational mesh, and to assign a random orientation for the direction of **N** for each nanodomain relative to **N** of the ''background'' antiferromagnetism $[\theta(\mathbf{r}) = \pm 120°]$. On a mesh of 160 $\times$160 points $(32\xi_\varepsilon \times 32\xi_\varepsilon)$ approximately 3400 nanodomains (nanodefects) are needed to cover all three orientations of the SBF equally. An example configuration of the AFM order appears in Fig. 9. In Fig. 10 we show a typical distribution of nanodefects on a mesh of $32\xi_\varepsilon \times 32\xi_\varepsilon$ with a concentration of defects that covers approximately 44% of the mesh. Each nanoscale defect has a cross-shaped five-point layout on the mesh. Interactions between adjacent defects or between clusters of defects were neglected. Figure 11 shows the specific heat as a function of temperature obtained by heating from deep in the low-temperature phase. Two phase transitions are signaled by heat-capacity jumps that remain sharp, consistent with second-order phase transitions, even in the presence of a high density of nanoscale defects. Increasing nanodomain density does lead to a reduction in the splitting of T_c and only a single phase transition is observed for a nanodomain density larger than $\sim$75%. The temperature evolution of the spatially averaged spontaneous magnetization shown in Fig. 11 indicates that the low-temperature transition that separates two superconducting states is second order. As expected, the rapid increase in the spontaneous magnetization is correlated with the appearance of a jump in the heat capacity, as shown in the top panel of Fig. 11. Note that time-reversal symmetry is broken for the single transition that occurs at high nanodomain densities.

In contrast to Model I, the contribution to the free energy from the symmetry-breaking field dominates that from the gradient term as reflected in the large ratios $\langle f_{\rm sbf}(\mathbf{r})\rangle_{\mathbf{r}} / \langle f_{\rm grad}(\mathbf{r})\rangle_{\mathbf{r}}$ shown in Fig. 12. The superconducting order parameter is on average aligned relative to the (background) AFM order except in a region $\sim\xi_\varepsilon$ around a nanodomain.

In Fig. 13 we compare our results of the specific heat with measurements on high-quality crystals. Since the heat jumps are very insensitive to the density of nanodomains, a wide range of ε values and nanodomain concentrations are consistent with experiments. In particular, an SBF coupling $\varepsilon/T_0 = 0.0633$ requires a concentration of roughly 36% in order to account for the observed sharp double transition in heat-capacity measurements.

It is natural to expect that disorder will drive the lower-temperature phase transition from being second order to first order or possibly a glass transition. Our numerical heating and cooling cycles have shown that upon heating up and crossing the low-temperature phase transition, the entropy is always smooth and hence the transition is second order. However, when starting the cooling cycle above T_{c-} we find

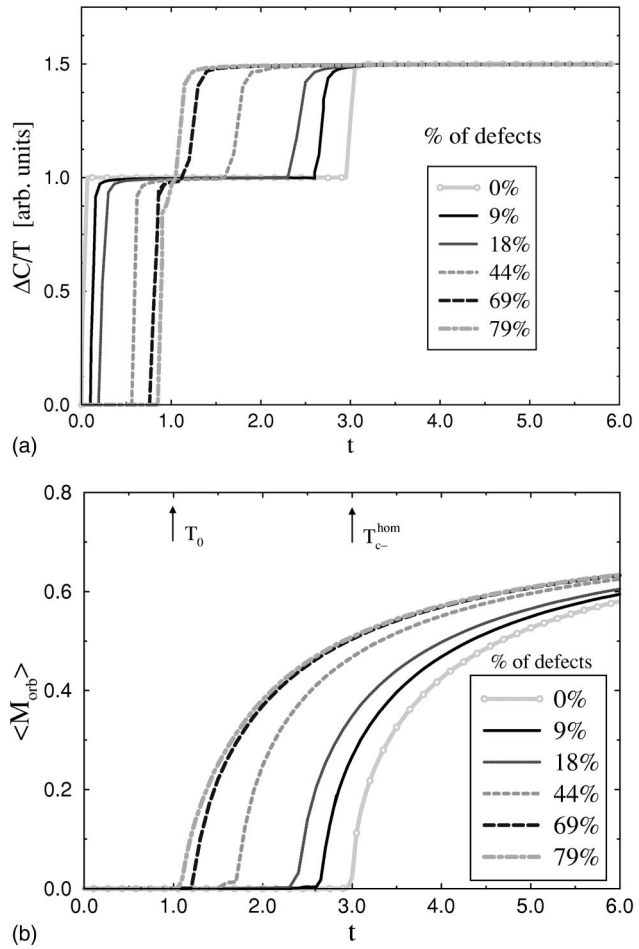

FIG. 11. Top: The specific heat for Model II in units of $\triangle C_+^{\mathrm{hom}}/T_{c+}^{\mathrm{hom}}$ for the nanoscale defect model for various defect densities on a $32\xi_\varepsilon \times 32\xi_\varepsilon$ lattice. Bottom: The orbital magnetization for the same model and set of parameters as in the top panel.

a glasslike, frustrated, and strongly disordered solution for the order parameter, which gives rise to a discontinuity in the entropy upon crossing T_{c-}. This discontinuity is consistent with a first-order transition. However, a comparison of the calculated free energies shows that the latter is energetically less favorable than the solution with a smooth transition and signals that the glasslike solution is metastable. Assuming that the metastable glasslike solution is experimentally observable when rapidly cooling down, our calculations give a small latent heat $l = T_{c-} \triangle S = \mu T_{c-} \triangle C_-$, where μ is a numerical factor of order $\mu \sim 0.01$. In other words, the latent heat is a small fraction of the overall measured specific heat $Q \approx T_{c+} C_N \approx 200$ mJ/mol, with $l/Q < 1\%$ or even less. In a carefully devised heat-capacity measurement this small latent heat should be observable if indeed a glasslike phase transition occurs.

IV. CONCLUSIONS

We have explored the effect of spatially inhomogeneous antiferromagnetic order coupled to the superconducting order parameter of an E_{2u} superconductor in two models representing limiting configurations of the AFM order parameter: Model I, abutting AFM domains of uniform size equally distributed over the three possible orientations of the AFM order parameter, and Model II, small domains with dimensions of the order of the superconducting coherence length (nanodomains), randomly dispersed through a single AFM domain. Our numerical solutions of the Ginzburg-Landau equations show that Model I is very sensitive to domain size. Phase transitions are rapidly broadened and

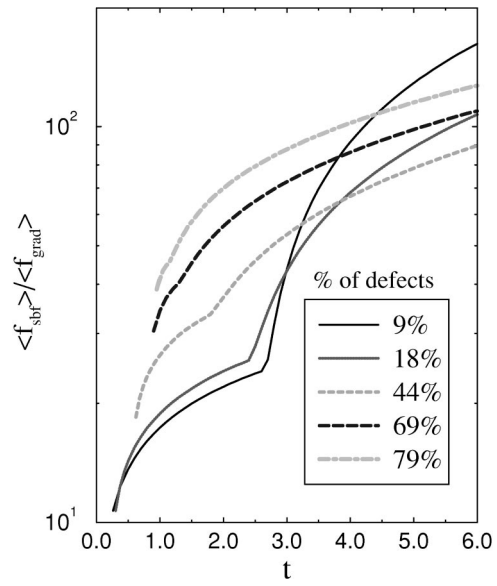

FIG. 12. The ratio of the contributions to the free energy from $\langle f_{\mathrm{sbf}}(\mathbf{r})\rangle_{\mathbf{r}}$ and $\langle f_{\mathrm{grad}}(\mathbf{r})\rangle_{\mathbf{r}}$. A large ratio reflects a stiff condensate; it is energetically less favorable for the superconducting order parameter to twist near the nanodomains. Note that the second transition can be described by $t_- \simeq \exp([1-x/x_{cr}]\ln 3)$, where $x_{cr} \approx 88\%$ is the critical concentration of nanoscale defects, where there is only one superconducting transition.

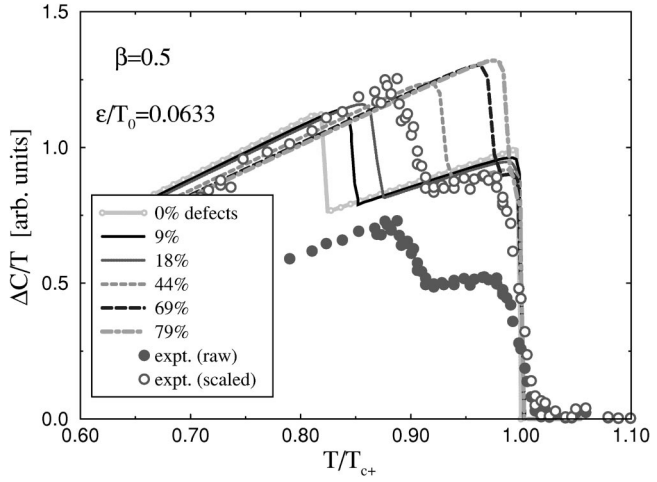

FIG. 13. Calculated specific heat as a function of temperature for Model II for various concentrations of nanodomains, shown in comparison with experiment (filled circles) normalized by C_N/T (Ref. 14). For ease of comparison, the experimental data scaled by a numerical factor (open circles) is also presented. The T dependence of the GL result has been corrected according to Fig. 7.

smeared as the domain size is decreased. For domain sizes less than $\sim 2\xi_\varepsilon$ only one transition is evident. The results of our calculations in two dimensions are in qualitative agreement with those of the simple one-dimensional model of Garg. In contrast, Model II shows sharp phase transitions for all nanodomain densities up to the point where the double phase transition gives way to a single phase transition. Our calculations for Model II show that low-lying metastable states affect the thermodynamic properties of the system as it is cooled, and suggest the possibility that the lower transition may be weakly first order. In contrast, our calculations for Model I show no evidence of a first-order transition. Although both models can yield sharp phase transitions like those observed in the heat capacities of high-quality samples, neither of them can account for the change in the heat capacity on annealing if the magnetic moments and domain sizes do not change as a result of annealing. The qualitative difference in the results for our two models does caution that simplistic models involving domains *homogeneous* in size do not rule out the possibility of E_{2u} superconductivity in UPt_3. The relative insensitivity of the low-temperature time-reversal symmetry-breaking phases to SIAFM in both models provides a natural explanation of how an E_{2u} superconductor can provide a good description of the gap structure of UPt_3 at low temperature and therefore transport properties that are in good agreement with experiment. In the temperature region that includes the two phase transitions, Model I appears to be too sensitive to SIAFM while Model II is perhaps not sensitive enough. It is, thus, more likely that SIAFM is not arranged in abutting domains of uniform size, but rather, there is a distribution of AFM domain sizes peaked around a particular size. Further calculations are required to properly consider this possibility, which we will examine in forthcoming work.

ACKNOWLEDGMENTS

We thank J.A. Sauls for enlightening discussions early in this work and P. Kumar and H. Röder for many stimulating discussions. M.J.G. acknowledges the support of Los Alamos National Laboratory under the auspices of the Department of Energy and D.W.H. acknowledges the support of the Office of Naval Research. This work was supported in part by a grant of computer time from the DoD High Performance Computing and Modernization Program on the Naval Research Laboratory's Origin 2000 and SUN Wildfire computers.

[1] G. Aeppli, E. Bucher, C. Broholm, J.K. Kjems, J. Baumann, and J. Hufnagl, Phys. Rev. Lett. **60**, 615 (1988).
[2] E.D. Isaacs, P. Zschack, C.L. Broholm, C. Burns, G. Aeppli, A.P. Ramirez, T.T.M. Palstra, R.W. Erwin, N. Stücheli, and E. Bucher, Phys. Rev. Lett. **75**, 1178 (1995).
[3] S.M. Hayden, L. Taillefer, C. Vettier, and J. Flouquet, Phys. Rev. B **46**, 8675 (1992).
[4] B.S. Adenwalla, S.W. Lin, Q.Z. Ran, Z. Zhao, J.B. Ketterson, J.A. Sauls, L. Taillefer, D.G. Hinks, M. Levy, and B.K. Sarma, Phys. Rev. Lett. **65**, 2298 (1990).
[5] G. Bruls, D. Weber, B. Wolf, P. Thalmeier, and B. Lüthi, Phys. Rev. Lett. **65**, 2294 (1990).
[6] M. Boukhny, G.L. Bullock, B.S. Shivaram, and D.G. Hinks, Phys. Rev. Lett. **73**, 1707 (1994); Phys. Rev. B **50**, 8985 (1994); D.S. Jin, S.A. Carter, B. Ellman, T.F. Rosenbaum, and D.G. Hinks, Phys. Rev. Lett. **68**, 1597 (1992).
[7] J.A. Sauls, Adv. Phys. **43**, 113 (1994).
[8] R.H. Heffner and M.R. Norman, Comments Condens. Matter Phys. **17**, 361 (1996).
[9] K. Machida, M. Ozaki, and T. Ohmi, J. Phys. Soc. Jpn. **58**, 4116 (1989).
[10] D.-C. Chen and A. Garg, Phys. Rev. Lett. **70**, 1689 (1993); A. Garg and D.-C. Chen, Phys. Rev. B **49**, 479 (1994).
[11] R. Heid, Ya.B. Bazaliy, V. Martisovits, and D.L. Cox, Phys. Rev. Lett. **74**, 2571 (1995).
[12] M.E. Zhitomirsky and K. Ueda, Phys. Rev. B **53**, 6591 (1996).
[13] A. Garg, J. Phys.: Condens. Matter **10**, 4223 (1998).
[14] R.J. Keizer, A. de Visser, M.J. Graf, A.A. Menovsky, and J.M. Franse, Phys. Rev. B **60**, 10 527 (1999).
[15] H. Tou, Y. Kitaoka, K. Asayama, N. Kimura, Y. Onuki, E. Yamamoto, and K. Maezawa, Phys. Rev. Lett. **77**, 1374 (1996); P. Dalmas de Réotier and A. Yaouanc, Phys. Lett. A **205**, 239 (1995); R.A. Fisher, B.F. Woodfield, S. Kim, N.E. Phillips, L. Taillefer, A.L. Giorgi, and J.L. Smith, Solid State Commun. **80**, 263 (1991); J.P. Vithayathil, D.E. Maclaughlin, E. Koster, D.L. Williams, and E. Bucher, Phys. Rev. B **44**, 4705 (1991); M. Lee, G.F. Moores, Y.Q. Song, W.P. Halperin, W.W. Kim, and G.R. Stewart, *ibid.* **48**, 7392 (1993).
[16] A. Yaouanc, P.D. de Reotier, F.N. Gygax, A. Schenck, A. Amato, C. Baines, P.C.M. Gubbens, C.T. Kaiser, A. de Visser, R.J. Keizer, and A. Huxley, Phys. Rev. Lett. **84**, 2702 (2000).
[17] A. Sulpice, P. Gandit, J. Chaussy, J. Flouquet, D. Jaccard, P. Lejay, and J.L. Tholence, J. Low Temp. Phys. **62**, 39 (1986).
[18] R.J. Keizer, A. de Visser, A.A. Menovsky, J.J.M. Franse, B. Fåk, and J.-M. Mignot, Phys. Rev. B **60**, 6668 (1999).
[19] B. Lussier, L. Taillefer, W.J.L. Buyers, T.E. Mason, and T. Peterson, Phys. Rev. B **54**, R6873 (1996).
[20] N.H. van Dijk, B. Fåk, L.P. Regnault, A. Huxley, and M-T. Fernández-Díaz, Phys. Rev. B **58**, 3186 (1998).
[21] J. Moreno and J.A. Sauls, Phys. Rev. B **63**, 024419 (2001).
[22] G.E. Volovik, J. Phys. C **21**, L221 (1988).
[23] D.W. Hess, T.A. Tokuyasu, and J.A. Sauls, J. Phys.: Condens. Matter **1**, 8135 (1989); Physica B **163**, 720 (1990).
[24] T.A. Tokuyasu, D.W. Hess, and J.A. Sauls, Phys. Rev. B **41**, 8891 (1990).
[25] R. Joynt, V.P. Mineev, G.E. Volovik, and M.E. Zhitomirsky, Phys. Rev. B **42**, 2014 (1990).
[26] E.I. Blount, C.M. Varma, and G. Aeppli, Phys. Rev. Lett. **64**, 3074 (1990).
[27] M.R. Norman, Physica C **194**, 203 (1992).
[28] I. Luk'yanchuk and M.E. Zhitomirsky, Physica C **206**, 373 (1993).

[29] K.A. Park and R. Joynt, Phys. Rev. B **53**, 12 346 (1996).
[30] K. Machida and M. Ozaki, Phys. Rev. Lett. **66**, 3293 (1991); T. Ohmi and K. Machida, *ibid.* **71**, 625 (1993); K. Machida, T. Nishira, and T. Ohmi, J. Phys. Soc. Jpn. **68**, 3364 (1999).
[31] A recent high-energy x-ray-scattering experiment, Ref. 49, claims that the original D_{6h} symmetry classification for UPt_3 is incorrect and that the correct crystal symmetry is trigonal. The D_{3h} symmetry group contains a single two-dimensional E representation. The GL theory for a superconducting order parameter that transforms like this representation is formally identical to the E_{2u} representation that we consider. The calculations we present here are applicable without modification to an E_u superconducting state of D_{3h}.
[32] M.J. Graf, S.-K. Yip, and J.A. Sauls, J. Low Temp. Phys. **102**, 367 (1996); **106**, 727(E) (1997); **114**, 257 (1999).
[33] M.J. Graf, S.-K. Yip, and J.A. Sauls, Physica B **280**, 176 (2000).
[34] C.H. Choi and J.A. Sauls, Phys. Rev. Lett. **66**, 484 (1991); Phys. Rev. B **48**, 13 684 (1993).
[35] M.J. Graf, S.-K. Yip, and J.A. Sauls, Phys. Rev. B **62**, 14 393 (2000).
[36] D.W. Hess, Physica B **194-196**, 1419 (1994).
[37] J.A. Sauls, Phys. Rev. B **53**, 8543 (1996).
[38] N. Keller, J.L. Tholence, A. Huxley, and J. Flouquet, Phys. Rev. Lett. **73**, 2364 (1994); **74**, 2148(E) (1995).
[39] V.P. Mineev, Physica B **171**, 138 (1991).
[40] M.J. Graf and D.W. Hess (unpublished).
[41] G. Aeppli and C. Broholm, in *Handbook on the Physics and Chemistry of Rare Earths*, edited by K.A. Gschneider, L. Eyring, G.H. Lander, and G.R. Choppin (Elsevier, New York, 1994), Vol. 19, p. 123.
[42] It is worth noting that Eq. (6) is by design traceless and does not include a possible coupling term proportional to $|\boldsymbol{\eta}|^2|\mathbf{N}|^2$. This term is implicitly absorbed into the definition of T_0, as has been done in Ref. 23. An explicit accounting of this term is not relevant to the central focus of this work and does not affect its conclusions. Since this term is important in determining the temperature dependence of $|\mathbf{N}|$ below the superconducting phase transition [see for example, the superconducting glass model of B. Kishore and P. Singh, Physica C **215**, 59 (1993)], such a term must be explicitly included in any self-consistent model of coupled E-representation superconductivity and AFM order. Such a program was carried out for the single-domain E-representation models of Ref. 29 to make a quantitative analysis of the H-P-T phase diagram. Our work suggests that a quantitative E-representation model of the H-P-T phase diagram should take the spatial dependence of the AFM order into account; one cannot assume that the equations of a single-domain model with ''renormalized couplings'' will be valid.
[43] J.A. Sauls, J. Low Temp. Phys. **95**, 153 (1994).
[44] J.P. Brison, N. Keller, P. Lejay, J.L. Tholence, A. Huxley, N. Bernhoeft, A.I. Buzdin, B. Fak, J. Flouquet, and L. Schmidt, J. Low Temp. Phys. **95**, 145 (1994).
[45] R.N. Kleiman, C. Broholm, G. Aeppli, E. Bucher, N. Stücheli, D.J. Bishop, K.N. Clausen, K. Mortensen, J.S. Pedersen, and B. Howard, Phys. Rev. Lett. **69**, 3120 (1992).
[46] Note that the specific-heat curves in Ref. 13 are labeled by a parameter that corresponds to the square of the domain size in our units.
[47] Small computational meshes may artificially suppress a transition to a glass phase.
[48] This phase is apparently not a glass, because $\langle \eta_i \rangle_{\mathbf{r}} \neq 0$ according to the Edwards-Anderson definition of a superconducting glass order parameter.
[49] D.A. Walko, J.-I. Hong, T.V.C. Rao, Z. Wawrzak, D.N. Seidman, W.P. Halperin, and M.J. Bedzyk, Phys. Rev. B **63**, 054522 (2001).
[50] P.A. Midgley, S.M. Hayden, L. Taillefer, B. Bogenberger, and H. von Löhneysen, Phys. Rev. Lett. **70**, 678 (1993).
[51] B.G. Demczyk, M.C. Aronson, B.R. Coles, and J.L. Smith, Philos. Mag. Lett. **67**, 85 (1993).